

Interaction between LiH molecule and Li atom from state-of-the-art electronic structure calculations

WOJCIECH SKOMOROWSKI, FILIP PAWŁOWSKI,

TATIANA KORONA, AND ROBERT MOSZYNSKI*

Faculty of Chemistry, University of Warsaw,

Pasteura 1, 02-093 Warsaw, Poland

PIOTR S. ŻUCHOWSKI AND JEREMY M. HUTSON

Department of Chemistry, Durham University,

South Road, Durham DH1 3LE, United Kingdom

* Author for correspondence; e-mail:robert.moszynski@tiger.chem.uw.edu.pl

Abstract

State-of-the-art *ab initio* techniques have been applied to compute the potential energy surface for the lithium atom interacting with the lithium hydride molecule in the Born-Oppenheimer approximation. The interaction potential was obtained using a combination of the explicitly correlated unrestricted coupled-cluster method with single, double, and noniterative triple excitations [UCCSD(T)–F12] for the core–core and core–valence correlation and full configuration interaction for the valence–valence correlation. The potential energy surface has a global minimum 8743 cm^{-1} deep if the Li–H bond length is held fixed at the monomer equilibrium distance or 8825 cm^{-1} deep if it is allowed to vary. In order to evaluate the performance of the conventional CCSD(T) approach, calculations were carried out using correlation-consistent polarized valence X -tuple-zeta basis sets, with X ranging from 2 to 5, and a very large set of bond functions. Using simple two-point extrapolations based on the single-power laws X^{-2} and X^{-3} for the orbital basis sets, we were able to reproduce the CCSD(T)–F12 results for the characteristic points of the potential with an error of 0.49% at worst. The contribution beyond the CCSD(T)–F12 model, obtained from full configuration interaction (FCI) calculations for the valence–valence correlation, was shown to be very small, and the error bars on the potential were estimated. At linear LiH–Li geometries the ground-state potential shows an avoided crossing with an ion-pair potential. The energy difference between the ground-state and excited-state potentials at the avoided crossing is only 94 cm^{-1} . Using both adiabatic and diabatic pictures we analyse the interaction between the two potential energy surfaces and its possible impact on the collisional dynamics. When the LiH bond is allowed to vary, a seam of conical intersections appears at C_{2v} geometries. At the linear LiH–Li geometry, the conical intersection is at a Li–H distance which is only slightly larger than the monomer equilibrium distance, but for nonlinear geometries it quickly shifts to Li–H distances that are well outside the classical turning points of the ground-state potential of LiH. This suggests that the conical intersection will have little impact on the dynamics of Li–LiH collisions at ultralow temperatures. Finally, the reaction channels for the exchange and insertion reactions are also analyzed, and found to be unimportant for the dynamics.

I. INTRODUCTION

Ultracold molecules offer new opportunities for scientific exploration, including studies of molecular Bose-Einstein condensates, novel quantum phases, and ultracold chemistry. For molecular interactions that take place at microKelvin temperatures, even the smallest activation energy exceeds the available thermal energy. This opens up new possibilities for controlling the pathways of chemical reactions (see, e.g., Ref. [1]).

A major objective of current experiments on cold molecules is to achieve quantum degeneracy, particularly for polar molecules. Two approaches are being pursued: indirect methods, in which molecules are formed from pre-cooled atomic gases, and direct methods, in which molecules are cooled from room temperature. There have been very substantial recent advances, particularly in indirect methods. In particular, the JILA [2] and Innsbruck [3] groups have formed deeply bound ground-state molecules at temperatures below $1 \mu\text{K}$, by magnetoassociation of pairs of ultracold atoms followed by coherent state transfer with lasers. Methods that form ultracold molecules from ultracold atoms are however restricted at present to species formed from heavy alkali-metal atoms.

Direct methods, such as buffer-gas cooling [4], Stark deceleration [5], crossed-beam collisional cooling [6] and Maxwell extraction [7], are applicable to a much larger variety of chemically interesting molecules. However, these methods cannot yet reach temperatures below 10 to 100 mK. Finding a way to cool these molecules further, below 1 mK, is one of the biggest challenges facing the field. The most promising possibility is so-called sympathetic cooling, in which cold molecules are introduced into an ultracold atomic gas and thermalize with it. Sympathetic cooling has been successfully used to achieve Fermi degeneracy in ^6Li [8] and Bose-Einstein condensation in ^{41}K [9], and for producing ultracold ions [10–12]. However, it has not yet been achieved for molecular systems, although there are theoretical proposals for experiments in which ultracold NH or ND₃ molecules are obtained by collisions with a bath of colder atoms such as Rb, Mg or N [13–15].

The group at Imperial College London recently succeeded in producing samples of cold LiH molecules in the first rotationally excited state [16, 17] using Stark deceleration. LiH is an attractive molecule for cooling, since it has large dipole moment and light mass, so that it can be controlled easily with fields. It has a relatively large rotational constant (7.5 cm^{-1}), which opens up the possibility of producing cold molecules in a single excited rotational state.

There is proposal to produce ultracold LiH molecules by sympathetic cooling with Li [18]. However, sympathetic cooling can be successful only if the rate of elastic (thermalization) collisions is large compared to the rate of inelastic (deexcitation) collisions, which cause trap loss. The main objects of the present paper are to explore the interaction between Li atoms and LiH molecules, to understand the nature of the interaction between these two species, and to obtain a detailed and accurate potential energy surface for the Li–LiH system.

The results of scattering calculations at ultralow temperature are very sensitive to the details of the interaction potential [13, 15]. For systems containing heavy atoms, the methods of quantum chemistry currently available cannot generate interaction potentials with accuracy better than a few percent. This limitation is caused by approximate treatments of correlation effects and relativistic contributions. With potential energy surfaces of moderate precision, it is usually possible to extract only qualitative information from low-energy collision calculations. By contrast, Li–LiH is a light system containing only 7 electrons and state-of-the-art *ab initio* electronic structure calculations can be performed with no significant approximations. It therefore offers a unique possibility to produce a very precise interaction potential, which will allow a quantitative description of Li–LiH collision dynamics, even in the ultralow temperature regime.

In electronic structure calculations one aims at approaching the exact solution of the Schrödinger equation, as closely as possible within the algebraic approximation. In practice, this is accomplished by combining hierarchies of one-electron and N -electron expansions. The accuracy increases across the hierarchies in a systematic manner, allowing the errors in the calculations to be controlled and a systematic approach to the the exact solution to be achieved. The standard N -electron hierarchy employed in electronic structure calculations consists of the Hartree-Fock (HF), second-order Møller-Plesset perturbation theory (MP2), coupled-cluster with single and double excitations (CCSD), and coupled-cluster with single, double, and approximate noniterative triple excitations [CCSD(T)] models, with the latter recovering most of the correlation energy. Thus, CCSD(T) constitutes a robust and accurate computational tool nowadays. All these models are size-consistent, which means that the interaction potential shows the correct dissociation behaviour at large intermolecular distances. In contrast, methods based on the configuration interaction approach with a restricted excitation space like multireference configuration interaction limited to single and double excitations (MRCISD) are not size-consistent and therefore they are not well suited

for calculations of the interaction energy.

The most popular example of a one-electron hierarchy is the family of Dunning correlation-consistent polarized valence basis sets, cc-pV_XZ [19] with the cardinal number X going from D (double-zeta), through T indicating triple-zeta, and so on. These have successfully been combined with the HF, MP2, CCSD, CCSD(T) hierarchy of wave function models for the calculation of various molecular properties [20–22]. The basis-set limit, corresponding to $X \rightarrow \infty$, may be approached either by extrapolating the results obtained with finite cardinal numbers towards infinite X [23, 24], or by replacing the standard one-electron hierarchy by explicitly-correlated methods, such as CCSD–F12 and CCSD(T)–F12 [25–30], in which the interelectron distance r_{12} is explicitly introduced into the wave function [31–33]. The F12 methods have recently been implemented efficiently [34–37] and shown to accelerate the convergence towards the basis-set limit for a number of properties [38–40].

In the present paper, we combine all-electron spin-unrestricted CCSD(T)–F12 calculations with frozen-core FCI calculations to yield a highly accurate best estimate of the Li–LiH interaction potential. We also compare the F12 interaction energies with results obtained from standard (not explicitly correlated) CCSD(T) calculations. We then characterize the ground-state potential, analyze possible interactions with excited states, and investigate channels for reactive collisions.

II. COMPUTATIONAL DETAILS

We have calculated the interaction energies between the lithium atom and the lithium hydride molecule in Jacobi coordinates (R, r, θ) , defined for the isotopic combination ⁷Li–⁷Li¹H. Calculations were performed for states of ²A' symmetry in the C_s point group. The LiH bond distance, r , was initially kept frozen at the LiH monomer equilibrium distance of 3.014 bohr [41]. The distance R between Li and the center of mass of LiH ranged from 3.0 to 10.0 bohr with an interval of 0.5 bohr, and then from 11.0 to 20.0 bohr with an interval of 1.0 bohr. Additional distances of 30.0, 40.0, and 50.0 bohr were also used. The angle θ , between the vector pointing from Li to H in the LiH molecule and the vector pointing from the center of mass of the molecule to the Li atom, was varied from 0° to 180° with an interval of 15°; $\theta = 0^\circ$ corresponds to Li–H—Li configurations. We thus used a total of 28 intermonomer distances, R , which combined with the 13 values of θ yielded 364 grid points

on the two-dimensional interaction energy surface.

Calculations with uncorrelated basis functions were carried out using the unrestricted version of the coupled-cluster model CCSD(T) with Dunning's cc-pV_XZ(-mid) basis sets with $X = D, T, Q, 5$, where mid indicates the inclusion of an additional set of basis functions, the so-called midbond-95 set [42], placed at the middle of the Li–LiH distance R . All electrons were correlated in these calculations. Additionally, for the purpose of comparison with the FCI results (see below), the frozen-core approximation ($1\sigma_{\text{LiH}}$ and $1s_{\text{Li}}$ orbitals kept frozen) was used for the cc-pVQZ basis. All these calculations were carried out using the MOLPRO package [43]. The full basis set of the dimer was used in the supermolecular calculations and the Boys and Bernardi scheme [44] was used to correct for basis-set superposition error.

The explicitly correlated spin-unrestricted CCSD–F12 and CCSD(T)–F12 [34, 35, 45, 46] calculations were carried out with the MOLPRO code [43] to establish the CCSD and CCSD(T) basis-set limits for the LiH–Li interaction. We chose to use the F12b variant [35, 46] of the explicitly correlated spin-unrestricted energy implemented in the MOLPRO code. Employing the fixed-amplitude ansatz for the F12 wave function ensured the orbital invariance and size-consistency of the CCSD-F12 and CCSD(T)-F12 results. The QZVPP basis set [47] was employed as the orbital basis in the F12 calculations. The corresponding QZVPP-jk basis set [48] was used as the auxiliary basis for the density-fitting approximation [45, 49] for many-electron integrals, while the uncontracted version of the QZVPP-jk basis was used to approximate the Resolution-of-Identity in the F12 integrals [50, 51]. In addition, the valence correlation in the dimer was described with the full configuration interaction method (FCI). The FCI and standard CCSD(T) calculations in the frozen-core approximation were carried out using the cc-pVQZ basis. The DALTON package [52] and the LUCIA program [53] were combined to yield the FCI results.

To calculate potential energy surface $V(R, \theta)$ with the LiH bond length kept fixed at its equilibrium value we used computational scheme which was previously applied in theoretical studies of the ground and excited states of the calcium dimer [54–58]. The potential $V(R, \theta)$ was constructed according to the following expression:

$$V(R, \theta) = V^{\text{CCSD(T)}-\text{F12}}(R, \theta) + \delta V_{\text{v-v}}^{\text{FCI}}(R, \theta) \quad (1)$$

where $V^{\text{CCSD(T)}-\text{F12}}(R, \theta)$ contribution was obtained from all-electron CCSD(T)-F12 calculations, while the correction for the valence-valence correlation beyond the CCSD(T)-F12 level,

$\delta V_{v-v}^{\text{FCI}}(R, \theta)$, was calculated in an orbital cc-pVQZ basis set. Both terms, $V^{\text{CCSD(T)}-\text{F}12}(R, \theta)$ and $\delta V_{v-v}^{\text{FCI}}(R, \theta)$, were obtained from the standard expressions for the supermolecule interaction energy, as given in Ref. [57].

The long-range asymptotic form of the potentials is of primary importance for cold collisions. We have therefore computed the leading long-range coefficients that describe the induction and dispersion interactions up to and including R^{-10} and $l = 4$ terms,

$$V(R, \theta) = - \sum_{n=6}^{10} \sum_{l=0}^{n-4} \frac{C_n^l}{R^n} P_l(\cos \theta), \quad (2)$$

where l is even/odd for n even/odd, and $C_n^l = C_n^l(\text{ind}) + C_n^l(\text{disp})$. The long-range coefficients $C_n^l(\text{ind})$ and $C_n^l(\text{disp})$ are given by the standard expressions (see, e.g., Refs. [59, 60]). The multipole moments and polarizabilities of LiH were computed with the recently introduced explicitly connected representation of the expectation value and polarization propagator within the coupled-cluster method [61–63], while the Li polarizabilities (both static and at imaginary frequencies) were taken from highly accurate relativistic calculations from Derevianko and coworkers [64].

The interaction potentials were interpolated between calculated points using the reproducing kernel Hilbert space method (RKHS) [65] with the asymptotics fixed using the *ab initio* long-range Van der Waals coefficients. The switching function of Ref. [66] was used to join the RKHS interpolation smoothly with the Van der Waals part in the interval between $R_a = 18$ and $R_b = 26$ bohr.

III. CONVERGENCE OF THE LI–LIH INTERACTION POTENTIAL TOWARDS THE EXACT SOLUTION

In sec. III A we analyze the convergence of the Li–LiH interaction potential with respect to the one-electron and N -electron hierarchies. Based on the analysis, we give in sec. III B our best estimate for the ground-state interaction potential with the Li–H bond length fixed at its monomer equilibrium value. The features of the potential are presented in sec. III C.

A. Convergence of the one-electron and N -electron hierarchies

In order to investigate the saturation of the Li–LiH interaction energy in the one-electron space, we have analyzed three characteristic points of the Li–LiH potential (the global minimum, the saddle point, the local minimum, and one point very close to the avoided crossing: $R = 5.5$ bohr and $\theta = 0.0^\circ$). The characteristic points were obtained from the potentials calculated at the CCSD(T) / cc-pV X Z-mid level of theory, for $X = D, T, Q$, and 5. The interaction energies were then compared to the corresponding energies of the spin-unrestricted CCSD(T)-F12 / QZVPP potential (approximation F12b), which serves as the basis-set limit. To evaluate the accuracy of the pure one-electron basis (*not* explicitly correlated), the relative percentage errors, $\Delta_{\text{F12b}} = (V^{\text{cc-pV}XZ} - V^{\text{F12b}}) / |V^{\text{F12b}}| \cdot 100\%$, were determined for each X at every characteristic point. The results are given in Table I.

We have also evaluated the characteristic points from the extrapolated interaction energy surfaces, which were generated as follows: at each grid point, the extrapolated *total* energies for Li, LiH, and Li–LiH were obtained by adding the Hartree-Fock energy calculated with cardinal number X to the extrapolated correlation energy, $E_{(X-1)X}^{\text{corr}}$, obtained from the two-point extrapolation formula [23, 24],

$$E_{(X-1)X}^{\text{corr}} = E_X^{\text{corr}} + \frac{E_X^{\text{corr}} - E_{(X-1)}^{\text{corr}}}{[1 - (X)^{-1}]^{-\alpha} - 1}, \quad (3)$$

where $E_{(X-1)}^{\text{corr}}$ and E_X^{corr} are the correlation energies obtained for two consecutive cardinal numbers, $(X - 1)$ and X , respectively. The final extrapolated interaction energy at a single grid point is obtained by subtracting the Li and LiH extrapolated total energies from the Li–LiH extrapolated total energy. We used the values $\alpha = 2$ and $\alpha = 3$, which were recommended by Jeziorska *et al.* in their helium dimer study [67, 68] as the ones most suited for extrapolating all the components of the interaction energy. The energies of the characteristic points obtained in this way were compared with the CCSD(T)-F12 / QZVPP results and the corresponding values of Δ_{F12b} are included in Table I.

The relative percentage errors, Δ_{F12b} , are plotted in Fig. 1 for both plain (non-extrapolated) and extrapolated characteristic points. For the global minimum, the plain cc-pV X Z results approach the basis-set limit from above and the convergence is smooth and fast: the error is reduced by a factor of 2 to 3 for each increment in X . The extrapolation accelerates the convergence: the $(X - 1)X$ extrapolated interaction energies have a quality

at least that of the plain cc-pV($X+1$)Z results. Though the extrapolation with $\alpha = 2$ seems to be more efficient than that with $\alpha = 3$ for the DT and TQ cases, it actually overshoots the basis-set limit when the Q and 5 cardinal numbers are used. More importantly, using $\alpha = 2$ leads to irregular behaviour: the Q5 extrapolation results in a lower quality than the TQ extrapolation. In contrast, extrapolation with $\alpha = 3$, though slightly less efficient for low cardinal numbers, exhibits highly systematic behaviour and leads to an error as small as 0.01% for the Q5 extrapolation.

Similar behaviour of the extrapolation schemes is observed for the point near the avoided crossing. Both extrapolations, with $\alpha = 2$ and $\alpha = 3$, converge smoothly towards the basis-set limit, but the convergence is not as fast as in the case of the global minimum. In contrast to the global minimum, there is no problem here with overshooting the basis-set limit. For each pair of cardinal numbers $(X-1)X$ the extrapolation with $\alpha = 2$ gives results slightly more favourable than using $\alpha = 3$, with the smallest error of 0.19% for the Q5 extrapolation.

For the saddle point and local minimum, the convergence of the relative errors is not as smooth as for the global minimum: the relative error for $X=D$ is surprisingly small. This is obviously accidental and does not reflect particularly high quality of the cc-pVDZ basis set. Indeed, when the cc-pVDZ results are employed in Eq. (3), the extrapolation worsens the accuracy: the errors for the DT extrapolation are much larger than the errors for both the $X=D$ and $X=T$ plain results, independent of the value of the α extrapolation parameter. Starting from $X=T$, the plain results smoothly approach the basis-set limit, though the convergence is clearly slower than in the case of the global minimum. The extrapolation with $\alpha = 2$ is unsystematic and unpredictable, as in the case of the global minimum, while that with $\alpha = 3$ smoothly approaches the basis-set limit. The errors of the Q5 extrapolation with $\alpha = 3$ are -0.49% for the saddle point and -0.13% for the local minimum.

Patkowski and Szalewicz [69] recently investigated Ar_2 with the CCSD(T)-F12 method. They found that the F12a and F12b variants [35] gave significantly different results. They also concluded that, for Ar_2 , calculations with explicitly correlated functions cannot yet compete with calculations employing extrapolation based on conventional orbital basis sets. Indeed, while their orbital results converged smoothly towards the extrapolated results, the CCSD(T)-F12a and CCSD(T)-F12b results behaved erratically with respect to both the orbital and the extrapolated results. Table I shows that this is not the case for the Li–LiH system. In our case the CCSD(T)-F12a and CCSD(T)-F12b results are quite similar and

are fully consistent with the plain and extrapolated results with conventional basis sets. It should be stressed, however, that Ar_2 is bound mostly by dispersion forces, while the main source of the bonding in $\text{Li}-\text{LiH}$ is the induction energy, which is less sensitive to the basis-set quality. This may at least partly explain the success of the CCSD(T)-F12 calculations for $\text{Li}-\text{LiH}$.

Finally, it is important to note here that, while the interaction energy at the characteristic points varies considerably with the basis set and extrapolation method, the positions of the points (i.e., the distance R and angle θ at which the characteristic points occur) remain practically unaffected by the choice of the basis set and extrapolation scheme.

To analyze the convergence of the CCSD and CCSD(T) models in the N -electron space, Fig. 2 compares the characteristic points (global minimum, saddle point, local minimum, and near the avoided crossing) of the $\text{Li}-\text{LiH}$ potential calculated at the CCSD / cc-pVQZ and CCSD(T) / cc-pVQZ levels of theory with the characteristic points obtained at the FCI / cc-pVQZ level. The $1\sigma_{\text{LiH}}$ and $1s_{\text{Li}}$ orbitals were kept frozen in the calculations. As expected, the N -electron error is reduced by a factor of 3 to 4 when the approximate triples correction is included in the calculations. It can also be seen from the figure that the global minimum is the most sensitive and the local minimum is the least sensitive to the description of the electron correlation.

B. The best estimate of the ground-state $\text{Li}-\text{LiH}$ potential energy surface

Because of the negligible one-electron error in the CCSD(T)-F12 calculations and to the rather large basis set used in the FCI / cc-pVQZ calculations, and assuming that the one-electron and N -electron errors are approximately independent, the best estimate of the ground-state interaction energy surface for the LiH-Li is

$$V^{\text{best}} = V^{\text{CCSD(T)-F12}} + \delta V_{\text{v-v}}^{\text{FCI}} + \delta V^{\text{FCI}}, \quad (4)$$

where $V^{\text{CCSD(T)-F12}}$ is the CCSD(T) basis-set limit energy (i.e., the CCSD(T)-F12 result) and the FCI correction, $\delta V_{\text{v-v}}^{\text{FCI}}$, is obtained by subtracting the CCSD(T) / cc-pVQZ energy from the FCI / cc-pVQZ energy, both calculated in the frozen-core approximation. The quantity δV^{FCI} accounts for the last remaining correction (in the non-relativistic limit), namely the effects of core-core and core-valence correlation in the FCI / cc-pVQZ calcula-

tions,

$$\delta V^{\text{FCI}} = \delta V_{\text{all-all}}^{\text{FCI}} - \delta V_{\text{v-v}}^{\text{FCI}}, \quad (5)$$

where the subscript “all” refers to all electrons correlated.

The quantity δV^{FCI} is a measure of the uncertainty in our best estimate V^{best} . To estimate this, we may safely assume that δV^{FCI} is at most as large as the corresponding $\delta V^{(\text{T})}$,

$$\delta V^{\text{FCI}} \leq \delta V^{(\text{T})} = \delta V_{\text{all-all}}^{(\text{T})} - \delta V_{\text{v-v}}^{(\text{T})}, \quad (6)$$

where

$$\delta V_{\text{all-all}}^{(\text{T})} = V_{\text{all-all}}^{\text{CCSD}(\text{T})} - V_{\text{all-all}}^{\text{CCSD}} \quad (7)$$

$$\delta V_{\text{v-v}}^{(\text{T})} = V_{\text{v-v}}^{\text{CCSD}(\text{T})} - V_{\text{v-v}}^{\text{CCSD}}, \quad (8)$$

with $V_{\text{all-all}}^{\text{CCSD}(\text{T})}$, $V_{\text{all-all}}^{\text{CCSD}}$, $V_{\text{v-v}}^{\text{CCSD}(\text{T})}$, and $V_{\text{v-v}}^{\text{CCSD}}$ denoting interaction energies calculated at the CCSD(T) / cc-pVQZ or CCSD / cc-pVQZ level, correlating all electrons or using the frozen-core approximation, as appropriate. As can be seen from Fig. 2, the differences between CCSD(T) and CCSD are, for the characteristic points of the potential, 2 to 3 times larger (and for the rest of the potential at least 1.5 times larger) than the differences between FCI and CCSD(T). Eq. (6) is therefore actually a conservative estimate for δV^{FCI} . The root mean square error for $\delta V^{(\text{T})}/\delta V_{\text{all-all}}^{(\text{T})}$, over the whole potential is 4.1%. We thus consider that our best estimate of the ground-state interaction energy for LiH–Li, Eq. (4), has a (conservative) total uncertainty of 5% of the FCI correction ($\delta V_{\text{v-v}}^{\text{FCI}}$). The analysis of the Li–LiH potential in the remainder of this paper is based on the interaction energies obtained using Eq. (4), unless otherwise stated.

To justify our error estimation we have performed calculations with all electron correlated at the FCI level for the set of characteristic points of the potential. Due to the immense memory requirements of the FCI calculations with seven electrons we were able to apply the cc-pVDZ basis set only. The FCI/cc-pVDZ results together with the CCSD(T)/cc-pVDZ, both with and without the frozen-core approximation, are presented in Table II. The error in the FCI correction calculated with frozen core is as small as 0.76 % for the examined points. We may see that the approximation with the FCI valence correction added to CCSD(T), Eq. (1), reproduces the exact FCI results with accuracy better than 1% of the FCI correction ($\delta V_{\text{v-v}}^{\text{FCI}}$). This confirms our estimate of 5% uncertainty in the FCI correction $\delta V_{\text{v-v}}^{\text{FCI}}$.

C. Features of the ground-state potential energy surface

In Table III we have listed the characteristic points of the potential energy surfaces of the ground state, which correlates at long range with $\text{Li}({}^2\text{S}) + \text{LiH}$ ($\text{X}^1\Sigma^+$), and the first excited state, which correlates at the long range with $\text{Li}({}^2\text{P}) + \text{LiH}$ ($\text{X}^1\Sigma^+$). Both these states are of ${}^2A'$ symmetry in the C_s point group. The latter is included in Table III since, as will be discussed in the next section, it shows an avoided crossing with the ground-state potential for the linear LiH–Li geometry. Table III shows that the interaction potential for the ground state of Li–LiH is deeply bound, with a binding energy of 8743 cm^{-1} at the global minimum. The global minimum is located at a skew geometry with $R_e=4.40$ bohr and $\theta_e=46.5^\circ$, and is separated by a barrier around $R=6.3$ bohr and $\theta=136.0^\circ$ from a shallow local minimum at the linear Li–LiH geometry. The local minimum is at $R=6.56$ bohr, with a well depth of only 1623 cm^{-1} . The excited-state potential shows only one minimum, at $R=5.66$ bohr, with a binding energy of 4743 cm^{-1} .

A contour plot of the ground-state potential is shown in the left-hand panel of Fig. 3, while the full-CI correction to the CCSD(T) potential, $\delta V_{\text{v-v}}^{\text{FCI}}$, is shown in the right-hand panel. The correction is very small compared to the best potential. It amounts to 0.4% around the global minimum, and approximately 1% at the local minimum. Thus, our estimated error of the calculation, 5% of the full-CI correction, translates into 0.05% error in the potential itself. We would like to reiterate here that such a small error was achieved not only because the interelectron distance was included explicitly in the *ab initio* CCSD(T)–F12 calculations, but also because of the very small valence-valence correlation beyond the CCSD(T) level. The smallness of the valence-valence correlation beyond the CCSD(T) level is not so surprising, since Li–LiH has only three valence electrons, and the exact model for a three-electron system would be CCSDT, coupled-cluster with single, double, and exact triple excitations [70]. Our results show that the triples contribution to the correlation energy beyond the CCSD(T) model for the valence electrons is very small.

The potential for the ground state of Li–LiH is very strongly anisotropic. This is easily seen in the left-hand panel of Fig. 3, and in Fig. 4, which shows the expansion coefficients of the potential in terms of Legendre polynomials $P_l(\cos \theta)$,

$$V(R, \theta) = \sum_{l=0}^{\infty} V_l(R) P_l(\cos \theta). \quad (9)$$

Here, $V_0(R)$ is the isotropic part of the potential and $\{V_l(R)\}_{l=1}^{\infty}$ is the set of anisotropic coefficients. Fig. 4 shows that, around the radial position of the global minimum, $R=4.36$ bohr, the first anisotropic contribution to the potential, $V_1(R)$, is far larger than the isotropic term, $V_0(R)$. The higher anisotropic components, with $l = 2, 3$, etc., contribute much less to the potential.

As mentioned above, calculations of collision dynamics at ultralow temperatures require accurate values of the long-range potential coefficients, Eq. (2). Some important scattering properties, such as the mean scattering length and the heights of centrifugal barriers, are determined purely by the Van der Waals coefficients. The calculated coefficients for Li–LiH are presented in Table IV. Because of the large dipole moment of lithium hydride and the relatively high polarizability of the lithium atom, the lowest-order, most important, coefficients are dominated by the induction contribution. For example, the induction part of C_6^0 and C_6^2 is 887 a.u., which accounts for 71% of C_6^0 and 98% of C_6^2 .

IV. INTERACTION BETWEEN THE GROUND AND EXCITED STATES

A. Low-lying excited state potential, nonadiabatic coupling matrix elements, and diabatic potentials

We encountered convergence problems with CCSD(T) calculations at the linear LiH–Li geometry around $R=5.6$ bohr, due to the presence of a low-lying excited state. The excited state correlates with the $\text{Li}({}^2\text{P}) + \text{LiH}(\text{X}^1\Sigma^+)$ dissociation limit, but closer investigation revealed that, at linear Li–HLi geometries near the crossing with the ground state, it has ion-pair character, $\text{Li}^+({}^1\text{S}) + \text{LiH}^-({}^2\Sigma)$. The ion-pair state itself has a crossing near $R = 9$ bohr with the lowest ${}^2A'$ state correlating with $\text{Li}({}^2\text{P}) + \text{LiH}(\text{X}^1\Sigma)$. This is shown schematically in Fig. 5. Away from linear Li–HLi geometries, the excited state has covalent character and remains below the ion-pair state all the way to dissociation. The avoided crossing between the ground state and the first excited state is at $R=5.66$ bohr, which is near the minimum of the ground-state potential at the linear geometry, and the energetic distance between the two states at the avoided crossing is only 94 cm^{-1} .

In order to investigate how far the excited state may affect the scattering dynamics, we computed the full potential energy surface for the excited state in question by means

of equation-of-motion coupled-cluster method with single and double excitations (EOM-CCSD) [71–73] implemented in the QCHEM code [74], using the orbital cc-pVQZ basis set. Cuts through the ground-state and excited-state potential energy surfaces at selected values of the angle θ are shown in Fig. 6. It may be seen that it is only near the linear LiH–Li geometry that the two states come very close together. If we distort the system from the linear geometry, the excited state goes up in energy very rapidly, and around the global minimum energy, $\theta \approx 45^\circ$, it is almost 6000 cm^{−1} above the ground state. The importance of the possible interaction between the ground and excited states can be measured by analyzing the (vectorial) nonadiabatic coupling matrix elements $\boldsymbol{\tau}_{12}$, defined as $\boldsymbol{\tau}_{12} = \langle \Psi_1 | \nabla \Psi_2 \rangle$, where ∇ is the gradient operator of the position vector and Ψ_1 and Ψ_2 are the wave functions of the two lowest states. On the two-dimensional surface, we may define radial $\tau_{12,R} = \langle \Psi_1 | \partial \Psi_2 / \partial R \rangle$ and angular $\tau_{12,\theta} = \langle \Psi_1 | \partial \Psi_2 / \partial \theta \rangle$ components of the vector $\boldsymbol{\tau}_{12}$. We evaluated $\boldsymbol{\tau}_{12}$ for all (R, θ) geometries by means of the multireference configuration interaction method limited to single and double excitations (MRCI) [75, 76], using the MOLPRO code [43]. The nonadiabatic coupling is largest when the two states are very close in energy, as it can be seen in Fig. 6. While at $\theta = 0^\circ$ the radial component of the nonadiabatic coupling approaches the Dirac delta form near the crossing point R_{ac} , with increasing angle it becomes a broad function of approximately Lorentzian shape. [Note the different scales on the vertical axes of the different panels.]

The transformation from the adiabatic representation to a diabatic representation may be expressed in terms of a mixing angle γ ,

$$H_1 = V_2 \sin^2 \gamma + V_1 \cos^2 \gamma, \quad H_2 = V_1 \sin^2 \gamma + V_2 \cos^2 \gamma, \quad H_{12} = (V_2 - V_1) \sin \gamma \cos \gamma, \quad (10)$$

where V_1 and V_2 are the ground-state and excited-state adiabatic potentials, H_1 and H_2 are the diabatic potentials, and H_{12} is the diabatic coupling potential. In principle, the mixing angle γ may be obtained by performing line integration of the nonadiabatic coupling $\boldsymbol{\tau}_{12}$,

$$\gamma(\mathbf{R}) = \gamma(\mathbf{R}_0) + \int_{\mathbf{R}_0}^{\mathbf{R}} \boldsymbol{\tau}_{12} \cdot d\mathbf{l}, \quad (11)$$

where \mathbf{R}_0 is the starting point of the integration. For polyatomic molecules, however, the mixing angle γ obtained by integrating this equation is non-unique due to the contributions from higher states. To circumvent the problem of path dependence, one may assume that we deal with an ideal two-state model.

In our case, however, the ion-pair surface $\text{Li}^+(^1\text{S})+\text{LiH}^-(^2\Sigma)$ shows another crossing at small angles and large distances, $\theta \leq 15^\circ$ and $R \approx 9$ bohr, with another excited-state potential that correlates with the $\text{Li}(^2\text{P})+\text{LiH}(^1\Sigma)$ dissociation limit. Thus a third state Ψ_3 comes into play and a two-state model is not strictly valid. The energy of the first excited state goes up very rapidly with the angle θ , and at the same time the contribution of the ion-pair configuration to the wave function of the first excited state, Ψ_2 , diminishes rapidly. Fortunately, the nonadiabatic coupling matrix elements between the two lower states τ_{12} and between the two higher states τ_{23} are well isolated. The maximum of τ_{12} is separated from the maximum of τ_{23} by more than 4 bohr; the locations of the crossing points between the surfaces for $\theta = 0$ are shown in Fig. 5. Moreover, the coupling τ_{13} between the ground state and the third state is negligible over the whole configurational space. Thus, following the discussion of Baer *et al.* [77] on the application of the two-state model, we conclude that the necessary conditions are fulfilled for the Li–LiH system. Due to the spatial separation of the nonadiabatic couplings τ_{12} and τ_{23} , using the diabatization procedure based on the two-state model is justified. It is worth noting that in our particular case we could not use the so-called quasi-diabatization procedure [78], since it is not possible to assign a single-reference wave function. This is due to the fact that the excited state shows admixture from the ion-pair state.

As the starting point of the integration in Eq. (11), we chose $R = 20$ bohr and $\theta = 0^\circ$ and followed a radial path along $\theta = 0^\circ$ and subsequently angular paths at constant R . The diabatic potentials were then generated according to Eqs. (10). Contour plots of the adiabatic, diabatic, and coupling potentials, and of the mixing angle γ , are presented as functions of R and θ in Fig. 7. We consider first the mixing angle γ , which is plotted in the bottom right-hand panel of Fig. 7. As expected, the mixing angle shows an accumulation point at $\theta = 0^\circ$ at a distance R corresponding to the closely avoided crossing between the ground and excited states. For $\theta = 180^\circ$, the mixing angle is non-negligible, even at large distances. The coupling potential H_{12} vanishes quite slowly with distance R , as R^{-3} . For the coupling between the ground and ion-pair states, this long-range decay is exponential, because of the different dissociation limits of the two surfaces. As expected, at large distances the two diabatic surfaces approach the respective adiabatic surfaces. The diabatic surface that correlates asymptotically with the excited-state $\text{Li}(^2\text{P})+\text{LiH}$ surface has an important contribution from the ground-state adiabatic potential only inside the avoided crossing and

at small angles θ . The diabatic surface that correlates asymptotically with the ground state resembles the ground-state adiabatic surface rather less closely, especially at large values of θ . The coupling between the diabatic states is small over a significant region of θ and LiH bond length r in the vicinity of the crossing. Physically, this means that the dynamics will be strongly nonadiabatic in this region, and to take this rigorously into account would require a full two-state treatment of the dynamics. However, there are no open channels that involve the second surface, and any collisions that cross onto it must eventually return to the original surface. Its effect in collision calculations will therefore be at most to cause a phase change in the outgoing wavefunction.

B. Conical intersection

It is well known that potential energy surfaces for homonuclear triatomic systems composed of hydrogen [79] or lithium atoms [80] show conical intersections at equilateral triangular geometries. Analogous behaviour may be expected for Li₂H, at geometries where the two lithium atoms are equivalent, i.e., C_{2v} geometries. Thus far, our discussion of the potential for Li–LiH has been restricted to two dimensions with the bond length of the LiH molecule fixed at its equilibrium value, and no conical intersection was observed. However, if we start to vary the bond length of the LiH molecule, conical intersections show up immediately.

At C_{2v} geometries, with the two LiH bond lengths equal, there are two low-lying electronic states, of 2A_1 and 2B_2 symmetries, that cross each other as a function of the internuclear coordinates. Fig. 8 shows contour plots of the two potential energy surfaces and of the difference between them, and the top panel of Fig. 9 summarizes some key features of the surfaces. The 2A_1 state has a minimum energy of -8825 cm^{-1} at $r(\text{LiH}) = 3.22$ bohr and an Li-H-Li angle of 95° . MRCI calculations with all coordinates free to vary confirm that this is indeed the absolute minimum geometry. There is also a saddle point on the 2A_1 surface at a linear H-Li-H geometry with $r(\text{LiH}) = 3.04$ bohr and an energy of -4992 cm^{-1} , which is a minimum in $D_{\infty h}$ symmetry. The 2B_2 state has a minimum energy of -5136 cm^{-1} at $r(\text{LiH}) = 3.17$ bohr at a linear Li-H-Li geometry. The 2A_1 saddle point and 2B_2 linear minimum have symmetries $^2\Sigma_g^+$ and $^2\Sigma_u^+$ respectively in $D_{\infty h}$ symmetry, but mix and distort if the constraint on the LiH bond lengths is relaxed, to form a $^2\Sigma^+$ state in $C_{\infty v}$ symmetry with a minimum at a linear geometry with $r(\text{LiH})$ distances of 3.00 and 3.33 bohr

and an energy of -5323 cm^{-1} . Even this is a saddle point with respect to bending on the full potential surface in C_s symmetry.

The $^2\text{A}_1$ and $^2\text{B}_2$ states are of different symmetries at C_{2v} geometries, but both are of $^2\text{A}'$ symmetry when the geometry is distorted from C_{2v} to C_s symmetry. The two states therefore mix and repel one another at geometries where the two LiH bond lengths are different, but a seam of conical intersections runs along the line where the energy difference is zero at C_{2v} geometries.

The fixed LiH distance used in previous sections ($r = 3.014$ bohr, shown as a dashed line on the figure) keeps the $^2\text{A}_1$ surface just below the $^2\text{B}_2$ surface. However, if we allow for the vibrations of LiH, the seam of conical intersections becomes accessible at near-linear LiH–Li geometries, where the zero of the energy difference appears for an Li–H distance only slightly larger than 3.014 bohr. At non-linear geometries the seam quickly moves to Li–H distances far outside the classical turning points of the ground vibrational level of free LiH, which are 2.72 and 3.35 bohr.

It is interesting to compare the features of the conical intersections in Li_2H with those in other triatomic molecules formed from Li and H atoms: LiH_2 , Li_3 and H_3 . In the case of LiH_2 , the seam of intersections occurs at highly bent C_{2v} geometries with an angle between the two Li–H bonds of approximately 30° and arises from degeneracy between the surfaces of A_1 and B_2 symmetry. The global minimum of B_2 symmetry is located at $r(\text{LiH}) = 3.23$ bohr and a bond angle H–Li–H of 28° [81]. This contrasts with Li_2H , where the minimum of B_2 symmetry is at a linear Li–H–Li configuration. The energy of the lowest point on the seam of intersections is about 9000 cm^{-1} above the $\text{Li}({}^2\text{S})+\text{H}_2(X^1\Sigma_g)$ threshold, so that it is irrelevant for low and medium-energy collisions between H_2 and Li in their ground states, though it is important for quenching of $\text{Li}({}^2\text{P})$ by H_2 [81, 82].

The conical intersections for the doublet states of Li_3 and H_3 occur at equilateral triangular geometries, where the ground state is doubly degenerate and has symmetry $^2\text{E}'$ in the D_{3h} point group. In the case of H_3 , the lowest-energy point on the seam is located at an energy more than 20000 cm^{-1} above the $\text{H}({}^2\text{S})+\text{H}_2(X^1\Sigma_g)$ threshold, so that nonadiabatic effects are negligible in $\text{H}+\text{H}_2$ collisions [83], although the conical intersection also produces geometric phase effects [84]. For Li_3 , the energetics are essentially different. The lowest-energy point on the seam is around 4000 cm^{-1} below the $\text{Li}({}^2\text{S})+\text{Li}_2(X^1\Sigma_g)$ threshold and only 500 cm^{-1} above the C_{2v} global minimum [85]. This is likely to produce considerable

nonadiabacity in collisions of Li_2 with Li.

To conclude, in all the triatomic molecules formed from H and Li there are seams of crossings that occur at configurations of the highest possible symmetry, either C_{2v} or D_{3h} . For Li_3 and Li_2H the conical intersections are accessible during atom-molecule collisions, while for H_3 and LiH_2 nonadiabatic processes are unimportant if the colliding partners are in their ground states and have relatively low kinetic energy.

V. REACTION CHANNELS

Several reaction channels exist that might affect sympathetic cooling [86] in $\text{Li}+\text{LiH}$. These are the exchange reaction,



and two insertion reactions,



producing $\text{Li}_2(\text{X}^1\Sigma_g^+)$ and $\text{Li}_2(a^3\Sigma_u^+)$ plus a ground-state H atom. The energetic location of the entrance and exit channels of these reactions, as well as those of the potential minima for linear and C_{2v} geometries, are shown in the upper panel of Fig. 9. The insertion reactions are highly endothermic, with an energy difference between the entrance and exit channels of the order of 12000 cm^{-1} and 22500 cm^{-1} for $\text{Li}_2(\text{X}^1\Sigma_g^+)+\text{H}$ and $\text{Li}_2(a^3\Sigma_u^+)+\text{H}$, respectively.

To make the discussion more quantitative, Fig. 9 also shows two-dimensional plots of the energy as functions of the internal coordinates. For the exchange reaction, we held $\text{Li}-\text{H}-\text{Li}$ at linear geometries and varied the distances from the two lithium atoms to the hydrogen atom. For the insertion reaction, $\text{Li}-\text{Li}-\text{H}$ was kept bent, with the angle $\angle(\text{HLi1Li2})$ held constant at the C_{2v} equilibrium value 42.5° , while the $\text{Li}-\text{Li}$ and $\text{Li}-\text{H}$ distances were varied. To make the plots consistent with the correlation diagram shown on the upper panel, the zero of energy was fixed at that of $\text{Li}-\text{LiH}$ separated to infinite distance with the $\text{Li}-\text{H}$ bond length fixed at the monomer equilibrium value.

Let us consider the exchange reaction first. The two-dimensional cut through the potential energy surface is presented in the left-hand panel of Fig. 9. The potential energy surface of linear Li_2H has two equivalent minima with an energy of -5323 cm^{-1} , separated by a small barrier 187 cm^{-1} high. The linear minima are in any case substantially above the

absolute minimum (8825 cm^{-1}), so this small barrier will have no important effect on the collision dynamics. The exchange reaction produces products that are indistinguishable from the reactants, so reactive collisions cannot be distinguished from inelastic collisions experimentally (unless the two Li atoms are different isotopes).

An analogous two-dimensional cut through the potential energy surface corresponding to $\text{Li}_2(\text{X}^1\Sigma_g)+\text{H}$ products is presented in the right-hand panel of Fig. 9. The plot illustrating the reaction to form $\text{Li}_2(a^3\Sigma_u)+\text{H}$ products is not reported, as the reaction is even more endothermic. The surface includes the absolute minimum at an energy of -8825 cm^{-1} . The entrance channel for this reaction corresponds to an Li–H distance of 3.014 bohr at large Li–Li distance, while in the exit channel the Li–Li distance is approximately 5.05 bohr when the Li–H distance is very large. However, this reaction cannot occur at low collision energies.

VI. SUMMARY AND CONCLUSIONS

In the present paper, state-of-the-art *ab initio* techniques have been applied to compute the ground-state potential energy surface for Li–LiH in the Born–Oppenheimer approximation. The interaction potential was obtained using a combination of the explicitly-correlated unrestricted coupled-cluster method with single, double, and approximate noniterative triple excitations [UCCSD(T)–F12] for the core–core and core–valence correlation, with full configuration interaction for the valence–valence correlation. The main results of this paper can be summarized as follows:

1. The Li–LiH system is strongly bound: if the LiH bondlength is held fixed at the monomer equilibrium distance of 3.014 bohr, the potential energy surface has a global minimum 8743 cm^{-1} deep at a distance $R=4.40$ bohr from the lithium atom to the center of mass of LiH, and a Jacobi angle $\theta = 46.5^\circ$. It also shows a weak local minimum 1623 cm^{-1} deep at the linear Li–LiH geometry for $R=6.56$ bohr, separated from the global minimum by a barrier at $R=6.28$ bohr and $\theta = 136^\circ$. If the LiH bond length is allowed to vary, the potential minimum is at a depth of 8825 cm^{-1} , at a C_{2v} geometry with LiH bond length of 3.22 bohr and an Li–H–Li angle of 95° .
2. The full-CI correction for the valence–valence correlation to the explicitly correlated CCSD(T)–F12 potential is very small. The remaining error in our calculations is due

to the neglect of the core–core and core–valence contributions, and is estimated to be of the order of 0.05% of the total potential.

3. To evaluate the performance of the conventional orbital electron-correlated methods, CCSD and CCSD(T), calculations were carried out using correlation-consistent polarized valence X -tuple zeta basis sets, with X ranging from D to 5, and a very large set of mid-bond functions. Simple two-point extrapolations based on the single-power laws X^{-2} and X^{-3} for the basis-set truncation error reproduce the CCSD(T)–F12 results for the characteristic points of the potential with an error of 0.49% at worst.
4. The potential for the ground state of Li–LiH is strongly anisotropic. Around the distance of the global minimum, the isotropic potential $V_0(R)$ is almost two times smaller than the first anisotropic contribution $V_1(R)$. Higher anisotropic components, with $l = 2, 3$, etc., do not contribute much to the potential.
5. At the linear LiH–Li geometry, the ground-state potential shows a close avoided crossing with the first excited-state potential, which has ion-pair character around the avoided crossing point. The full potential energy surface for the excited state was obtained with the equation-of-motion method within the framework of coupled-cluster theory with single and double excitations. The excited-state potential has a single minimum 4743 cm^{-1} deep for the linear LiH–Li geometry at $R=5.66$ bohr. The energy difference between the ground and excited states at the avoided crossing is only 94 cm^{-1} . An analysis of the nonadiabatic coupling matrix elements suggests that dynamics in the vicinity of the avoided crossing will have nonadiabatic character.
6. When stretching the LiH bond in the Li–LiH system, a seam of conical intersections appears for C_{2v} geometries, between the ground state of 2A_1 symmetry and an excited state of 2B_2 symmetry. At the linear LiH–Li geometry, the conical intersection occurs for an Li–H distance which is only slightly larger than the equilibrium distance of the LiH monomer, but for significantly non-linear geometries it moves to Li–H distances far outside the classical turning points of LiH.
7. The Li–LiH system has several possible reaction channels: an exchange reaction to form products identical to the reactants, and two insertion reactions that produce $\text{Li}_2(a^3\Sigma_u^+)$ and $\text{Li}_2(X^1\Sigma_g^+)$ plus a ground-state hydrogen atom. The insertion reactions

are highly endothermic, with the energy difference between the entrance and exit channels of the order of 12000 cm^{-1} and 22500 cm^{-1} for $\text{Li}_2(\text{X}^1\Sigma_g^+)+\text{H}$ and $\text{Li}_2(a^3\Sigma_u^+)+\text{H}$, respectively.

In a subsequent paper [87] we will analyze the dynamics of Li–LiH collisions at ultralow temperatures, based on our best *ab initio* potential. We will analyze the impact of the present inaccuracies in the *ab initio* electronic structure calculations, and discuss the prospects of sympathetic cooling of lithium hydride by collisions with ultracold lithium atoms.

Acknowledgments

We would like to thank Dr. Michał Przybytek for his invaluable technical help with the FCI calculations. We acknowledge the financial support from the Polish Ministry of Science and Higher Education (grant 1165/ESF/2007/03) and from the Foundation for Polish Science (FNP) via Homing program (grant HOM/2008/10B) within EEA Financial Mechanism. We also thank EPSRC for support under collaborative project CoPoMol of the ESF EUROCORES Programme EuroQUAM.

-
- [1] R. V. Krems, *Phys. Chem. Chem. Phys.* **10**, 4079 (2008).
 - [2] K.-K. Ni, S. Ospelkaus, M. H. G. de Miranda, A. Pe'er, B. Neyenhuis, J. J. Zirbel, S. Kotochigova, P. S. Julienne, D. S. Jin, and J. Ye, *Science* **322**, 231 (2008).
 - [3] J. G. Danzl, M. J. Mark, E. Haller, M. Gustavsson, R. Hart, J. Aldegunde, J. M. Hutson, and H.-C. Nägerl, *Nature Physics* **6**, 265 (2010).
 - [4] J. D. Weinstein, R. de Carvalho, T. Guillet, B. Friedrich, and J. M. Doyle, *Nature* **395**, 148 (1998).
 - [5] H. L. Bethlem, G. Berden, and G. Meijer, *Phys. Rev. Lett.* **83**, 1558 (1999).
 - [6] M. S. Eliooff, J. J. Valentini, and D. W. Chandler, *Science* **302**, 1940 (2003).
 - [7] L. D. van Buuren, C. Sommer, M. Motsch, M. S. S. Pohle, J. Bayerl, P. W. H. Pinkse, and G. Rempe, *Phys. Rev. Lett.* **102**, 033001 (2009).
 - [8] B. DeMarco and D. S. Jin, *Science* **285**, 1703 (1999).
 - [9] G. Modugno, G. Ferrari, G. Roati, R. J. Brecha, A. Simoni, and M. Inguscio, *Science* **294**, 1320 (2001).
 - [10] C. Zipkes, S. Palzer, C. Sias, and M. Köhl, *Nature* **464**, 388 (2010).
 - [11] C. Zipkes, S. Palzer, L. Ratschbacher, C. Sias, and M. Köhl.
 - [12] S. Schmid, A. Härter, J. Hecker Denschlag, and A. Frisch, private communication.
 - [13] P. S. Żuchowski and J. M. Hutson, *Phys. Rev. A* **79**, 062708 (2009).
 - [14] P. Soldán, P. S. Żuchowski, and J. M. Hutson, *Faraday Discuss.* **142**, 191 (2009).
 - [15] A. O. G. Wallis and J. M. Hutson, *Phys. Rev. Lett.* **103**, 183201 (2009).
 - [16] S. K. Tokunaga, J. O. Stack, J. J. Hudson, B. E. Sauer, E. A. Hinds, and M. R. Tarbutt, *J. Chem. Phys.* **126**, 12431 (2007).
 - [17] S. K. Tokunaga, J. M. Dyne, E. A. Hinds, and M. R. Tarbutt, *New Journal of Physics* **11**, 055038 (2009).
 - [18] M. Tarbutt, private communication (2008).
 - [19] T. H. Dunning, Jr., *J. Chem. Phys.* **90**, 1007 (1989).
 - [20] W. Klopper, K. L. Bak, P. Jørgensen, J. Olsen, and T. Helgaker, *J. Phys. B* **32**, R103 (1999).
 - [21] D. E. Woon and T. H. Dunning, Jr., *J. Chem. Phys.* **100**, 2975 (1994).
 - [22] K. L. Bak, J. Gauss, T. Helgaker, P. Jørgensen, and J. Olsen, *Chem. Phys. Lett.* **319**, 563

(2000).

- [23] K. L. Bak, A. Halkier, P. Jørgensen, J. Olsen, T. Helgaker, and W. Klopper, *J. Mol. Struct.* **567**, 375 (2001).
- [24] T. Helgaker, W. Klopper, H. Koch, and J. Noga, *J. Chem. Phys.* **106**, 9639 (1997).
- [25] T. Shiozaki, M. Kamiya, S. Hirata, and E. F. Valeev, *J. Chem. Phys.* **129**, 071101 (2008).
- [26] T. Shiozaki, M. Kamiya, S. Hirata, and E. F. Valeev, *Phys. Chem. Chem. Phys.* **10**, 3358 (2008).
- [27] A. Köhn, G. W. Richings, and D. P. Tew, *J. Chem. Phys.* **129**, 201103 (2008).
- [28] D. P. Tew, W. Klopper, C. Neiss, and C. Hättig, *Phys. Chem. Chem. Phys.* **9**, 1921 (2007).
- [29] D. Bokhan, S. Ten-no, and J. Noga, *Phys. Chem. Chem. Phys.* **10**, 3320 (2008).
- [30] D. P. Tew, W. Klopper, and C. Hättig, *Chem. Phys. Lett.* **452**, 326 (2008).
- [31] W. Kutzelnigg, *Theor. Chim. Acta* **68**, 445 (1985).
- [32] W. Klopper and W. Kutzelnigg, *Chem. Phys. Lett.* **134**, 17 (1987).
- [33] S. Ten-no, *Chem. Phys. Lett.* **398**, 56 (2004).
- [34] C. Hättig, D. P. Tew, and A. Kohn, *J. Chem. Phys.* **132**, 231102 (2010).
- [35] T. B. Adler, G. Knizia, and H.-J. Werner, *J. Chem. Phys.* **127**, 221106 (2007).
- [36] H.-J. Werner, T. B. Adler, G. Knizia, and F. R. Manby, in *Recent Progress In Coupled Cluster Method*, edited by P. Cársky, J. Paldus, and J. Pittner (Springer, Heidelberg, 2010).
- [37] D. P. Tew, C. Hättig, R. A. Bachorz, and W. Klopper, in *Recent Progress In Coupled Cluster Method*, edited by P. Cársky, J. Paldus, and J. Pittner (Springer, Heidelberg, 2010).
- [38] J. Yang and C. Hättig, *J. Chem. Phys.* **131**, 074102 (2009).
- [39] C. Neiss and C. Hättig, *J. Chem. Phys.* **126**, 154101 (2007).
- [40] J. Yang and C. Hättig, *J. Chem. Phys.* **130**, 124101 (2009).
- [41] G. Plummer, E. Herbst, and F. DeLucia, *J. Chem. Phys.* **81**, 4893 (1984).
- [42] H. Partridge and C. W. Bauschlicher Jr., *Mol. Phys.* **96**, 705 (1999).
- [43] H.-J. Werner, P. J. Knowles, R. Lindh, F. R. Manby, M. Schütz, P. Celani, T. Korona, A. Mitrushenkov, G. Rauhut, T. B. Adler, et al., *Molpro, version 2008.3, a package of ab initio programs* (2008), see <http://www.molpro.net>.
- [44] S. F. Boys and F. Bernardi, *Mol. Phys.* **19**, 553 (1970).
- [45] G. Knizia and H.-J. Werner, *J. Chem. Phys.* **128**, 154103 (2008).
- [46] G. Knizia, T. B. Adler, and H.-J. Werner, *J. Chem. Phys.* **130**, 054104 (2009).

- [47] F. Weigend and R. Ahlrichs, *Phys. Chem. Chem. Phys.* **7**, 3297 (2005).
- [48] F. Weigend, *J. Comp. Chem.* **29**, 167 (2008).
- [49] H. J. Werner, T. B. Adler, and F. R. Manby, *J. Chem. Phys.* **126**, 164102 (2007).
- [50] W. Klopper and C. C. M. Samson, *J. Chem. Phys.* **116**, 6397 (2002).
- [51] E. F. Valeev, *Chem. Phys. Lett.* **395**, 190 (2004).
- [52] T. Helgaker, H. J. A. Jensen, P. Jørgensen, J. Olsen, K. Ruud, H. Ågren, A. A. Auer, K. L. Bak, V. Bakken, O. Christiansen, et al., DALTON, *an ab initio electronic structure program, Release 2.0* (2005), see <http://www.kjemi.uio.no/software/dalton/dalton.html>.
- [53] LUCIA, *a general active space program by J. Olsen, with contributions from H. Larsen and M. Fülscher.*
- [54] B. Bussery-Honvault, J.-M. Launay, and R. Moszynski, *Phys. Rev. A* **68**, 032718 (2003).
- [55] B. Bussery-Honvault, J.-M. Launay, and R. Moszynski, *Phys. Rev. A* **72**, 012702 (2005).
- [56] B. Bussery-Honvault, J.-M. Launay, T. Korona, and R. Moszynski, *J. Chem. Phys.* **125**, 114315 (2006).
- [57] B. Bussery-Honvault and R. Moszynski, *Mol. Phys.* **104**, 2387 (2006).
- [58] C. P. Koch and R. Moszynski, *Phys. Rev. A* **78**, 043417 (2008).
- [59] B. Jeziorski, R. Moszynski, and K. Szalewicz, *Chem. Rev.* **94**, 1887 (1994).
- [60] R. Moszynski, in *In: Molecular Materials with Specific Interactions – Modeling and Design*, edited by W. A. Sokalski (Springer, New York, 2007), pp. 1–157.
- [61] B. Jeziorski and R. Moszynski, *Int. J. Quantum Chem.* **48**, 161 (1993).
- [62] R. Moszynski, P. S. Żuchowski, and B. Jeziorski, *Coll. Czech. Chem. Commun.* **70**, 1109 (2005).
- [63] T. Korona, M. Przybytek, and B. Jeziorski, *Mol. Phys.* **104**, 2303 (2006).
- [64] A. Derevianko, S. G. Porsev, and J. F. Babb, *At. Data Nucl. Data Tables* **96**, 323 (2010).
- [65] T.-S. Ho and H. Rabitz, *J. Chem. Phys.* **104**, 2584 (1996).
- [66] L. M. C. Janssen, G. C. Groenenboom, A. van der Avoird, P. S. Żuchowski, and R. Podeszwa, *J. Chem. Phys.* **131**, 224314 (2009).
- [67] M. Jeziorska, R. Bukowski, W. Cencek, M. Jaszunski, B. Jeziorski, and K. Szalewicz, *Coll. Czech. Chem. Commun.* **68**, 463 (2003).
- [68] M. Jeziorska, W. Cencek, K. Patkowski, B. Jeziorski, and K. Szalewicz, *Int. J. Quantum Chem.* **108**, 2053 (2008).
- [69] K. Patkowski and K. Szalewicz, *J. Chem. Phys.* **133**, 094304 (2010).

- [70] J. Noga and R. J. Bartlett, *J. Chem. Phys.* **86**, 7041 (1987).
- [71] H. J. Monkhorst, *Int. J. Quantum Chem. Symp.* **11**, 421 (1977).
- [72] H. Sekino and R. J. Bartlett, *Int. J. Quantum Chem. Symp.* **18**, 255 (1984).
- [73] J. F. Stanton and R. J. Bartlett, *J. Chem. Phys.* **98**, 7029 (1993).
- [74] Y. Shao, L. Fusti-Molnar, Y. Jung, J. Kussmann, C. Ochsenfeld, S. T. Brown, A. T. B. Gilbert, L. V. Slipchenko, S. V. Levchenko, D. P. O'Neill, et al., *Phys. Chem. Chem. Phys.* **8**, 3172 (2006).
- [75] H.-J. Werner and P. J. Knowles, *J. Chem. Phys.* **89**, 5803 (1988).
- [76] P. J. Knowles and H.-J. Werner, *Chem. Phys. Lett.* **145**, 514 (1988).
- [77] M. Baer, A. M. Mebel, and G. D. Billing, *J. Phys. Chem. A* **106**, 6499 (2002).
- [78] D. Simah, B. Hartke, and H.-J. Werner, *J. Chem. Phys.* **111**, 4523 (1999).
- [79] R. Abrol, A. Shaw, A. Kuppermann, and D. R. Yarkony, *J. Chem. Phys.* **115**, 4640 (2001).
- [80] D. A. Brue, X. Li, and G. A. Parker, *J. Chem. Phys.* **123**, 091101 (2005).
- [81] E. S. Kryachko and D. R. Yarkony, *Theor. Chem. Acc.* **100**, 154 (1998).
- [82] T. J. Martinez, *Chem. Phys. Lett.* **272**, 139 (1997).
- [83] T.-S. Chu, K.-L. Han, M. Hankel, G. G. Balint-Kurti, A. Kuppermann, and R. Abrol, *J. Chem. Phys.* **130**, 144301 (2009).
- [84] J. C. Juanes-Marcos and S. C. Althorpe, *J. Chem. Phys.* **122**, 204324 (2005).
- [85] A. I. Voronin, J. M. C. Marques, and A. J. C. Varandas, *J. Phys. Chem. A* **102**, 6057 (1998).
- [86] P. S. Źuchowski and J. M. Hutson, *Phys. Rev. A* **81**, 060703 (2010).
- [87] S. K. Tokunaga, W. Skomorowski, P. S. Źuchowski, R. Moszynski, J. M. Hutson, E. A. Hinds, and M. R. Tarbutt, to be published.

TABLE I: Performance of various orbital basis sets and extrapolation schemes compared to the CCSD(T)-F12a and CCSD(T)-F12b results at the characteristic points of the ground state potential energy surface of Li–LiH. The notation VXZ with X=D, T, Q, and 5 denotes the result of the orbital CCSD(T) calculations in the cc-pVXZ basis with midbond-95 set, XY α with X and Y = D, T, Q, and 5, and α = 2 or 3 denote the extrapolated result according to Eq. (3), while F12a and F12b stand for the explicitly correlated CCSD(T) results with the a and b approximation schemes. Δ_{F12a} and Δ_{F12b} are the percent error of given result with respect to the CCSD(T)-F12a and CCSD(T)-F12b results, respectively.

	V (cm $^{-1}$)	Δ_{F12a}	Δ_{F12b}	V (cm $^{-1}$)	Δ_{F12a}	Δ_{F12b}	V (cm $^{-1}$)	Δ_{F12a}	Δ_{F12b}	V (cm $^{-1}$)	Δ_{F12a}	Δ_{F12b}
	Global Minimum			Saddle point			Local minimum			Avoided crossing		
VDZ	-8547.77	1.87	1.84	-1548.64	-0.39	-0.61	-1616.54	-0.65	-0.77	-4771.50	4.59	4.65
VTZ	-8652.38	0.67	0.64	-1566.01	-1.52	-1.73	-1629.62	-1.46	-1.59	-4892.57	2.17	2.23
VQZ	-8683.85	0.31	0.27	-1555.93	-0.86	-1.08	-1618.22	-0.75	-0.88	-4955.39	0.91	0.97
V5Z	-8698.84	0.14	0.10	-1551.91	-0.60	-0.82	-1612.70	-0.41	-0.53	-4974.35	0.53	0.60
DT2	-8683.31	0.32	0.28	-1575.59	-2.14	-2.36	-1637.22	-1.94	-2.06	-4934.30	1.33	1.40
TQ2	-8704.14	0.08	0.04	-1541.85	0.05	-0.17	-1601.47	0.29	0.17	-4983.15	0.36	0.42
Q52	-8714.77	-0.05	-0.08	-1543.21	-0.04	-0.25	-1601.76	0.27	0.15	-4991.70	0.19	0.25
DT3	-8668.66	0.48	0.45	-1571.05	-1.84	-2.06	-1633.62	-1.71	-1.84	-4914.53	1.73	1.79
TQ3	-8695.37	0.18	0.14	-1547.94	-0.35	-0.56	-1608.71	-0.16	-0.28	-4971.14	0.60	0.66
Q53	-8707.24	0.03	0.01	-1546.78	-0.27	-0.49	-1606.24	-0.01	-0.13	-4984.59	0.33	0.39
F12a	-8710.85	0.00	-0.04	-1542.60	0.00	-0.21	-1606.14	0.00	-0.12	-5001.10	0.00	0.06
F12b	-8707.77	0.04	0.00	-1539.31	0.21	0.00	-1604.17	0.12	0.00	-5004.15	-0.06	0.00

TABLE II: Performance of the valence-valence FCI correction $\delta V_{v-v}^{\text{FCI}}$ against exact FCI results for the characteristic points of the LiH–Li potential (in cm^{-1}). Calculations were done in the cc-pVDZ basis set. Subscript all-all refers to all electrons correlated, while v-v denotes frozen-core results. Δ is the percentage error of the $\delta V_{v-v}^{\text{FCI}}$ approximation with respect to the $\delta V_{\text{all-all}}^{\text{FCI}}$:

$$\Delta = \frac{\delta V_{v-v}^{\text{FCI}} - \delta V_{\text{all-all}}^{\text{FCI}}}{|\delta V_{\text{all-all}}^{\text{FCI}}|} \cdot 100\%.$$

	GM	SP	LM	AC
$V_{v-v}^{\text{CCSD(T)}}$	-7553.16	-1407.50	-1502.25	-3785.91
V_{v-v}^{FCI}	-7587.86	-1437.27	-1522.05	-3806.93
$\delta V_{v-v}^{\text{FCI}}$	-34.70	-29.77	-19.80	-21.02
$V_{\text{all-all}}^{\text{CCSD(T)}}$	-7590.40	-1415.56	-1509.04	-3842.01
$V_{\text{all-all}}^{\text{FCI}}$	-7625.07	-1445.32	-1528.78	-3863.46
$\delta V_{\text{all-all}}^{\text{FCI}}$	-34.67	-29.76	-19.74	-21.45
$\Delta[\%]$	-0.09	-0.04	-0.30	0.76

TABLE III: Characteristic points of the interaction potentials for the ground state $\text{Li}({}^2\text{S}) + \text{LiH}$ ($\text{X}^1\Sigma^+$) and the first excited state, which correlates asymptotically with $\text{Li}({}^2\text{P}) + \text{LiH}$ ($\text{X}^1\Sigma^+$).

	R [bohr]	θ [degrees]	V [cm^{-1}]
Ground state			
Global minimum	4.40	46.5°	-8743
Local minimum	6.56	180.0°	-1623
Saddle point	6.28	136.0°	-1565
Excited state			
Global minimum	5.66	0.0°	-4743

TABLE IV: Long-range coefficients (in atomic units) for Li–LiH, from perturbation theory. Numbers in parentheses indicate powers of 10.

$l \rightarrow$	0	1	2	3	4
C_6^l	1247.8		869.7		
C_7^l		8304.2		2902.3	
C_8^l	4.83(4)		4.24(4)		8923.0
C_9^l		3.94(5)		6.42(4)	
C_{10}^l	2.03(6)		2.02(6)		2.44(5)

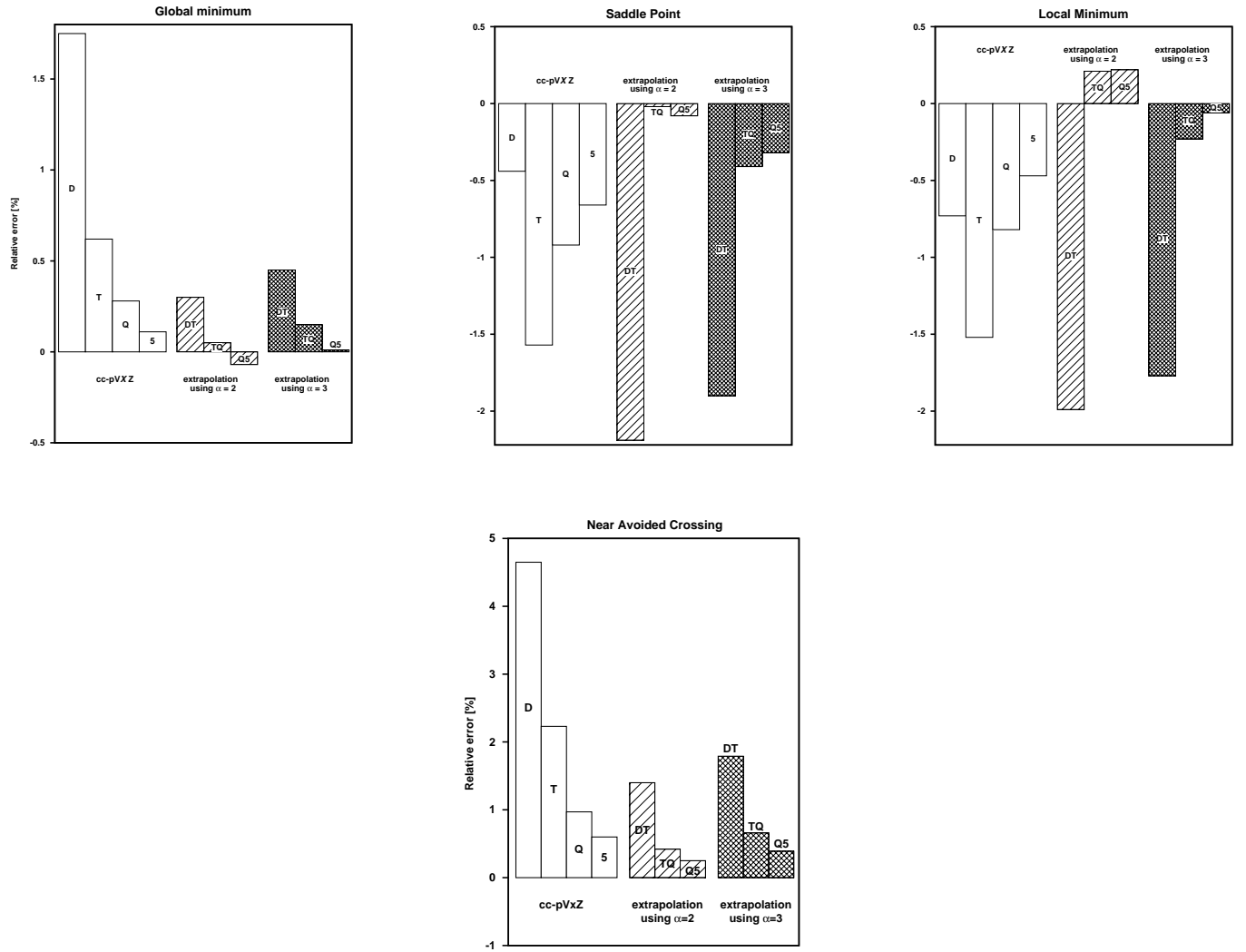


FIG. 1: Relative percentage errors of the interaction energy at the characteristic points (global minimum, saddle point, local minimum, and near the avoided crossing: $R=5.5$ bohr and $\theta = 0^\circ$) of the LiH-Li potential calculated at the CCSD(T) / cc-pVXZ-mid level, where $X = D, T, Q, 5$ and mid stands for the midbond-95 set. The errors for the characteristic points obtained by extrapolating the plain basis-set results with the two-point extrapolation formula are also shown for $\alpha = 2$ and $\alpha = 3$. The errors were obtained by comparison with the CCSD(T)-F12b / QZVPP results.

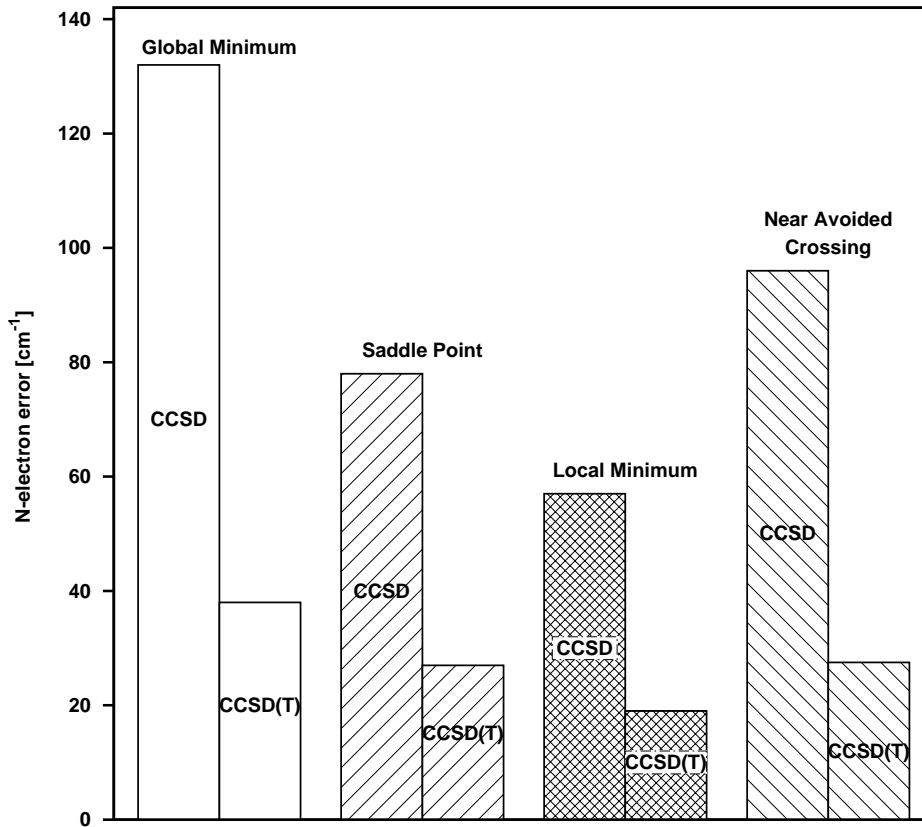


FIG. 2: The N -electron error of the characteristic points of the LiH–Li interaction potential calculated at the CCSD / cc-pVQZ and CCSD(T) / cc-pVQZ levels of theory. The error was determined by comparison with the FCI / cc-pVQZ interaction potential. The $1\sigma_{\text{LiH}} 1s_{\text{Li}}$ frozen-core approximation was used.

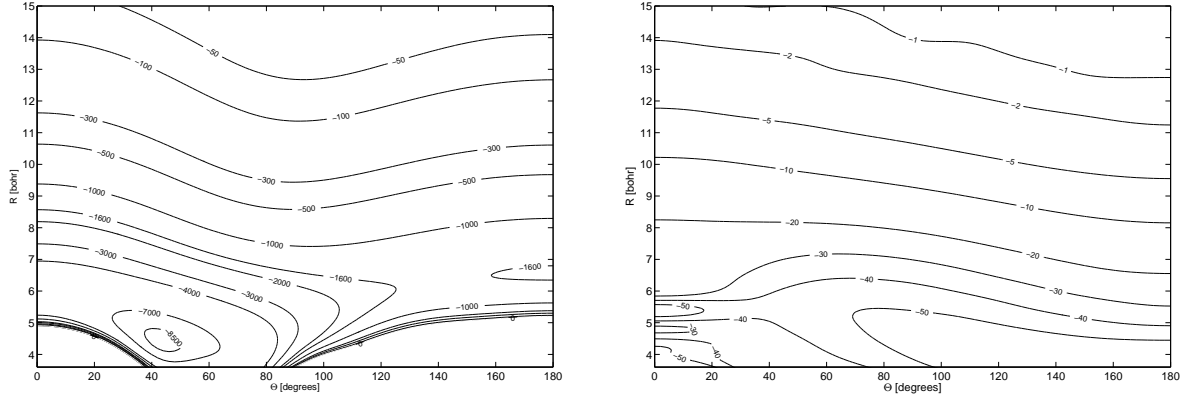


FIG. 3: Contour plots of the best *ab initio* potential for the ground state of Li–LiH (left-hand panel), and of the full-CI correction to the CCSD(T)–F12 potential (right-hand panel). Energies are in cm^{-1} .

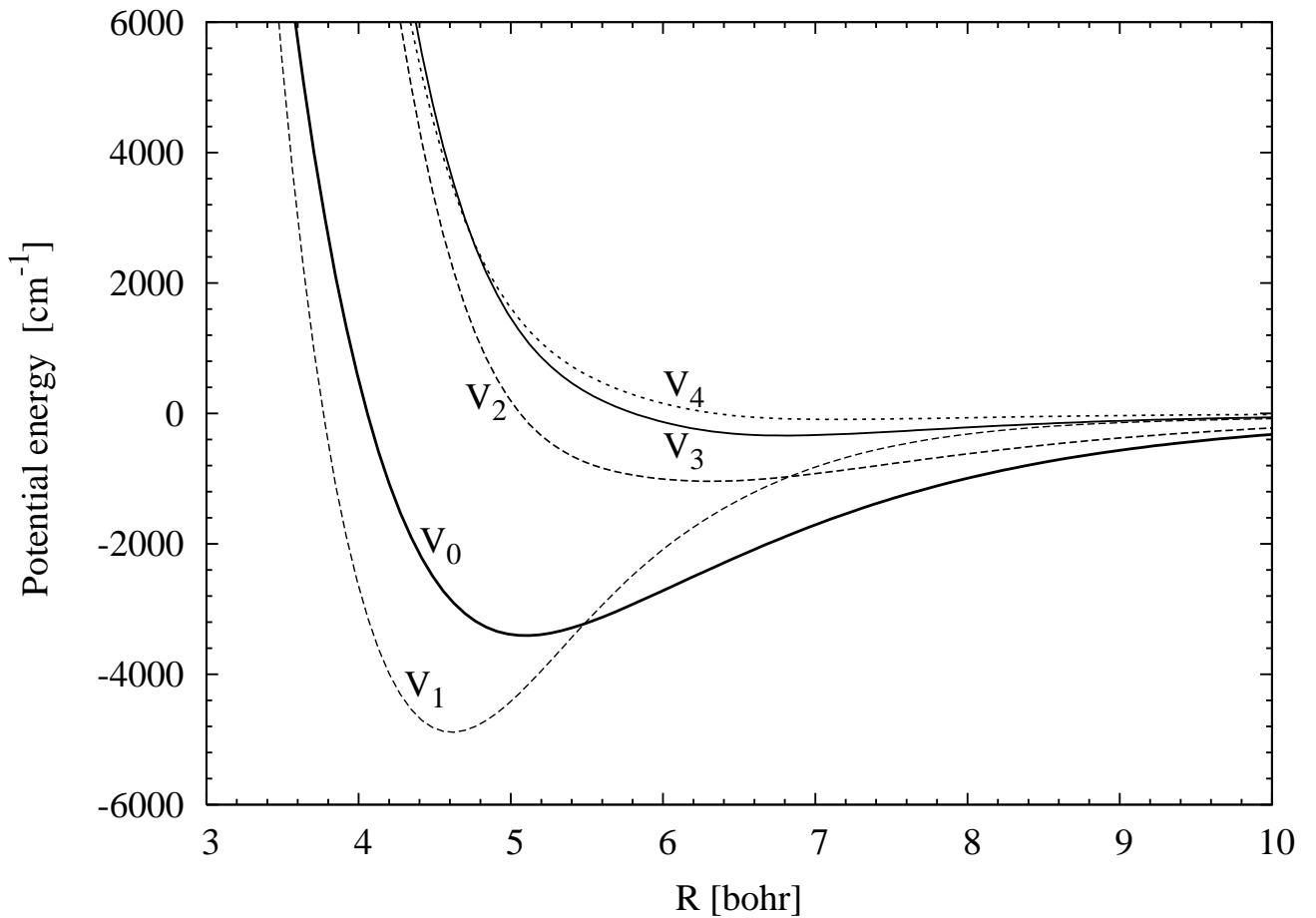


FIG. 4: The Legendre components $V_l(R)$ ($l = 0, 1, 2, 3, 4$) of the ground-state $\text{Li}(^2\text{S}) + \text{LiH}$ ($\text{X } ^1\Sigma^+$) interaction potential, see Eq. (9).

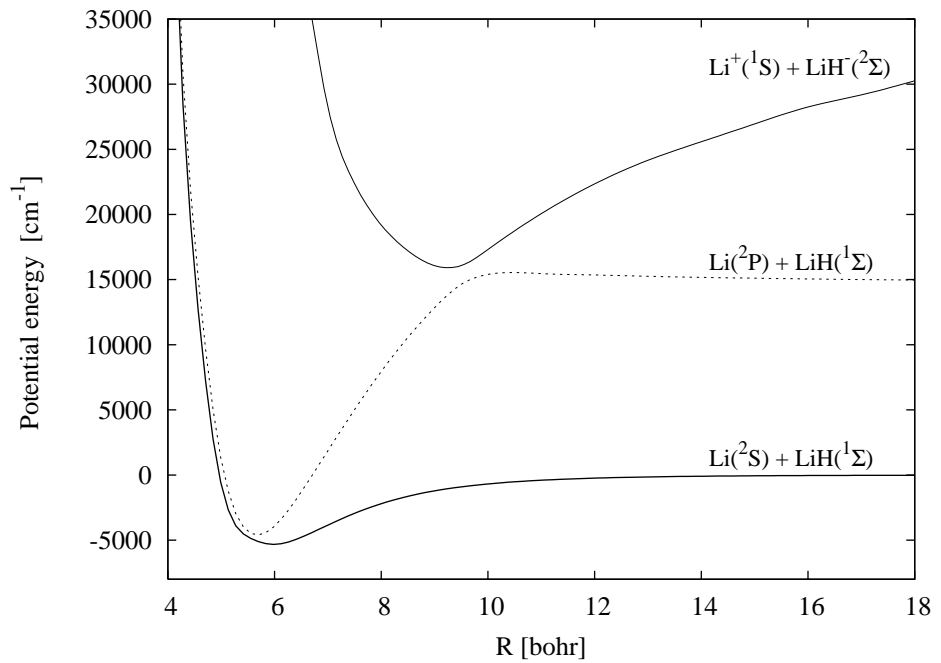


FIG. 5: Ground-state and excited-state potentials at the linear geometry LiH–Li: demonstration of the ion-pair nature of the excited-state potential.

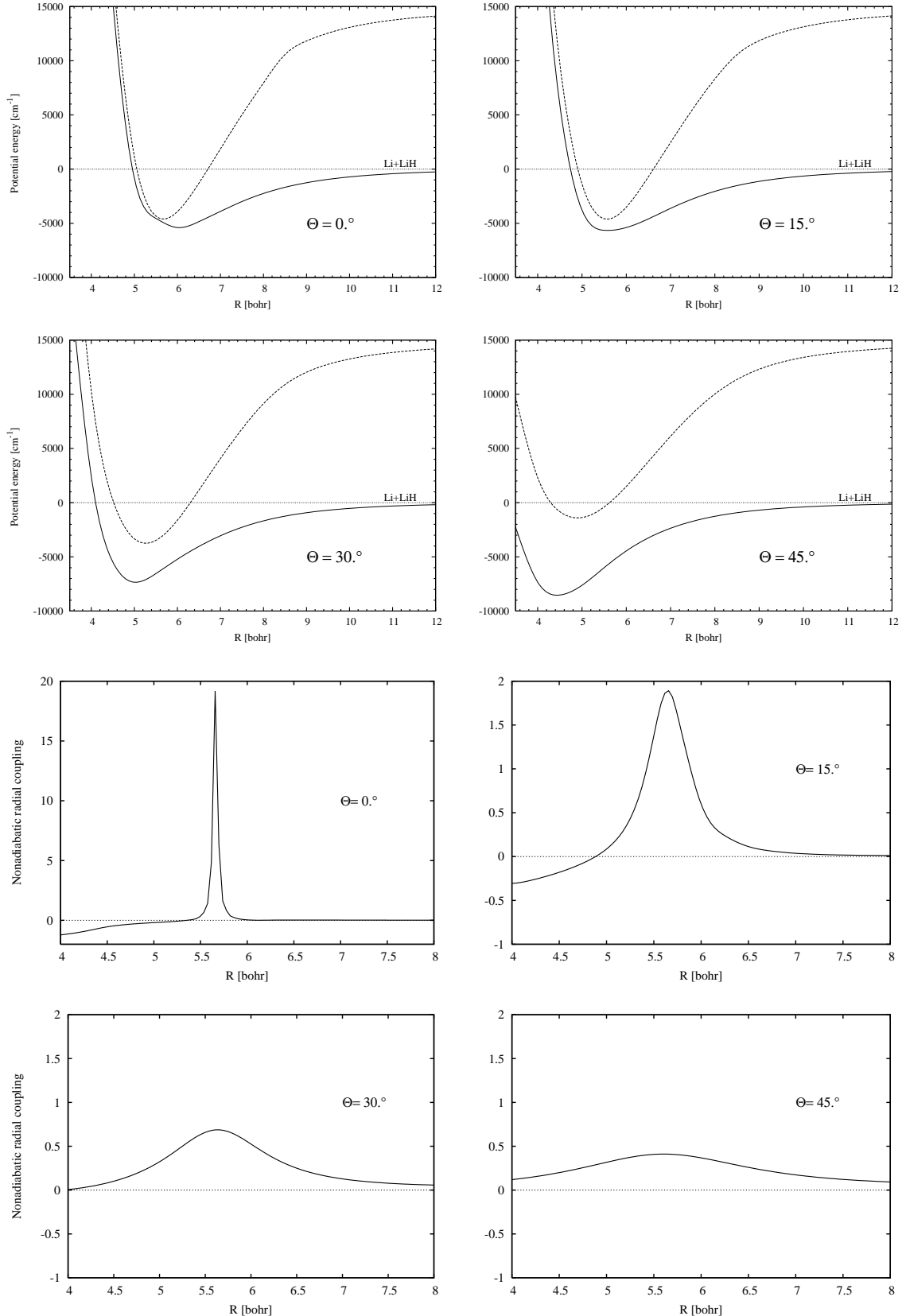


FIG. 6: Cuts through the potential energy surfaces for the ground and the first excited states of $^2A'$ symmetry for selected values of the angle θ , and the corresponding radial nonadiabatic coupling matrix elements as functions of the distance R .³⁵

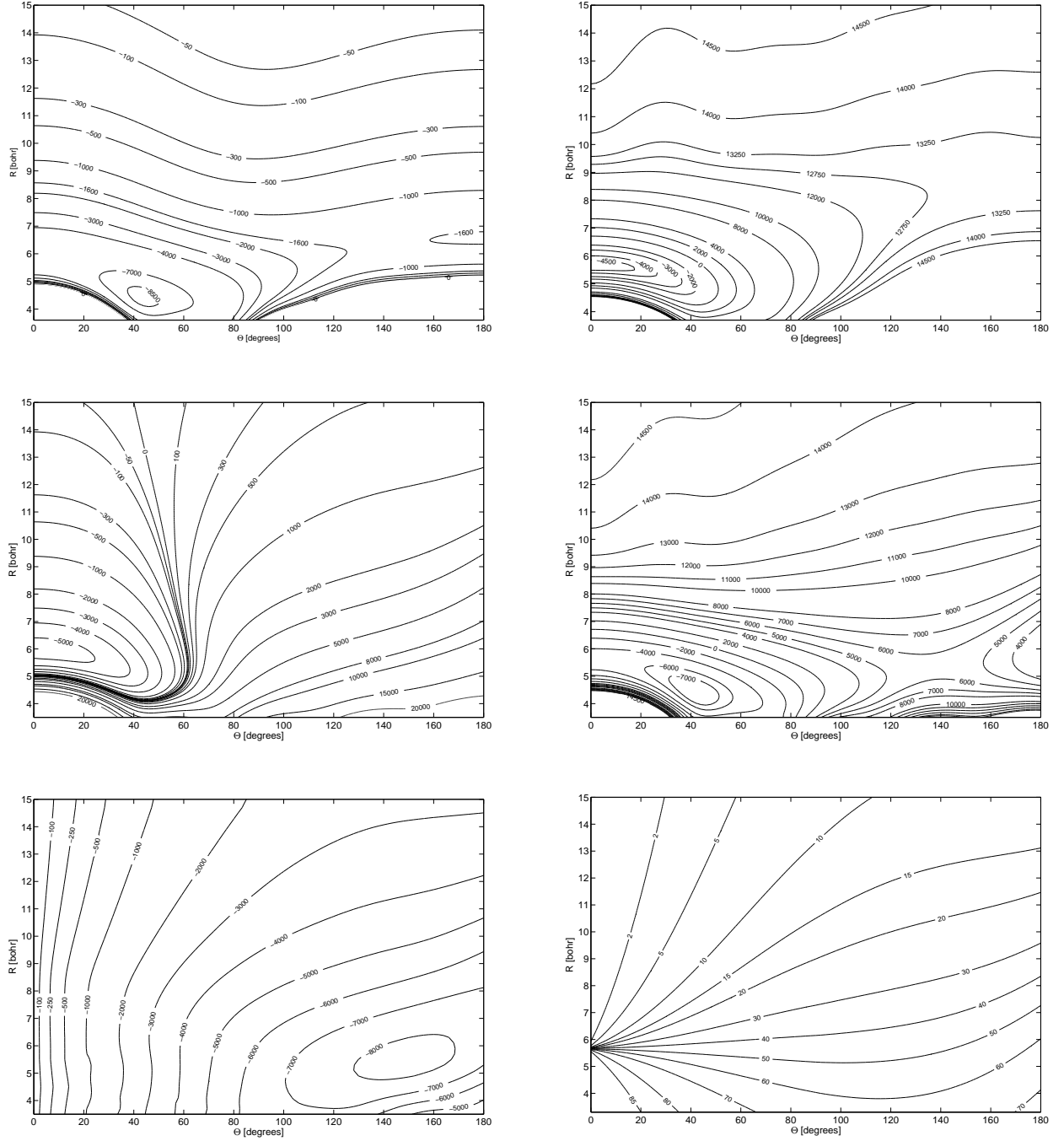


FIG. 7: Adiabatic potentials (top two panels), diabatic potentials (middle two panels), and coupling potential (bottom left-hand panel), and the mixing angle γ (bottom right-hand panel), as functions of the geometrical parameters R and θ . Energies are in cm⁻¹.

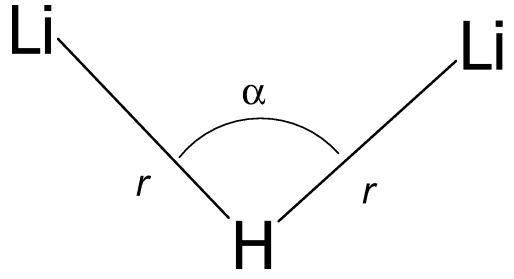
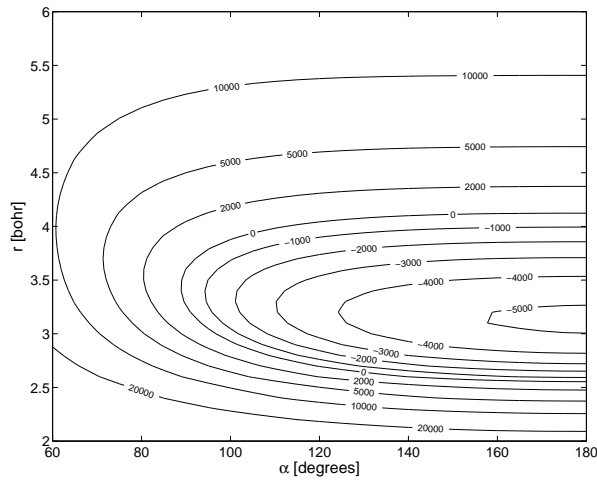
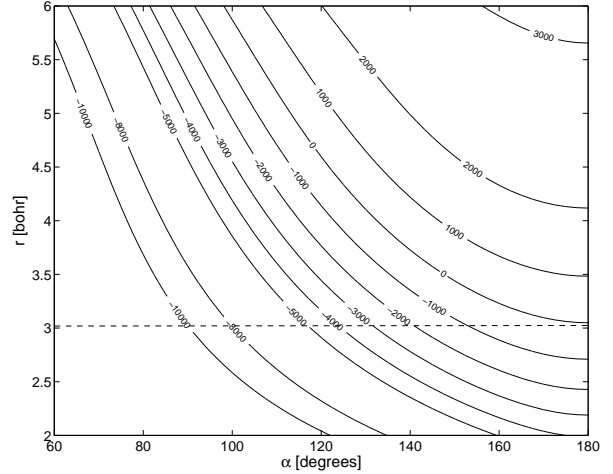
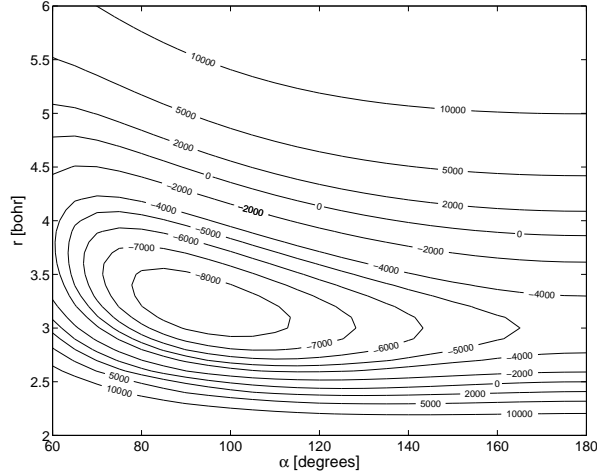


FIG. 8: Potential energy surfaces for the $^2\text{A}_1$ (top left-hand panel) and $^2\text{B}_2$ (bottom left-hand panel) states of Li_2H in C_{2v} symmetry, and the difference between them (top right-hand panel), which is zero along the seam of conical intersections. Also shown is the coordinate system used for C_{2v} geometries. Energies are in cm^{-1} .

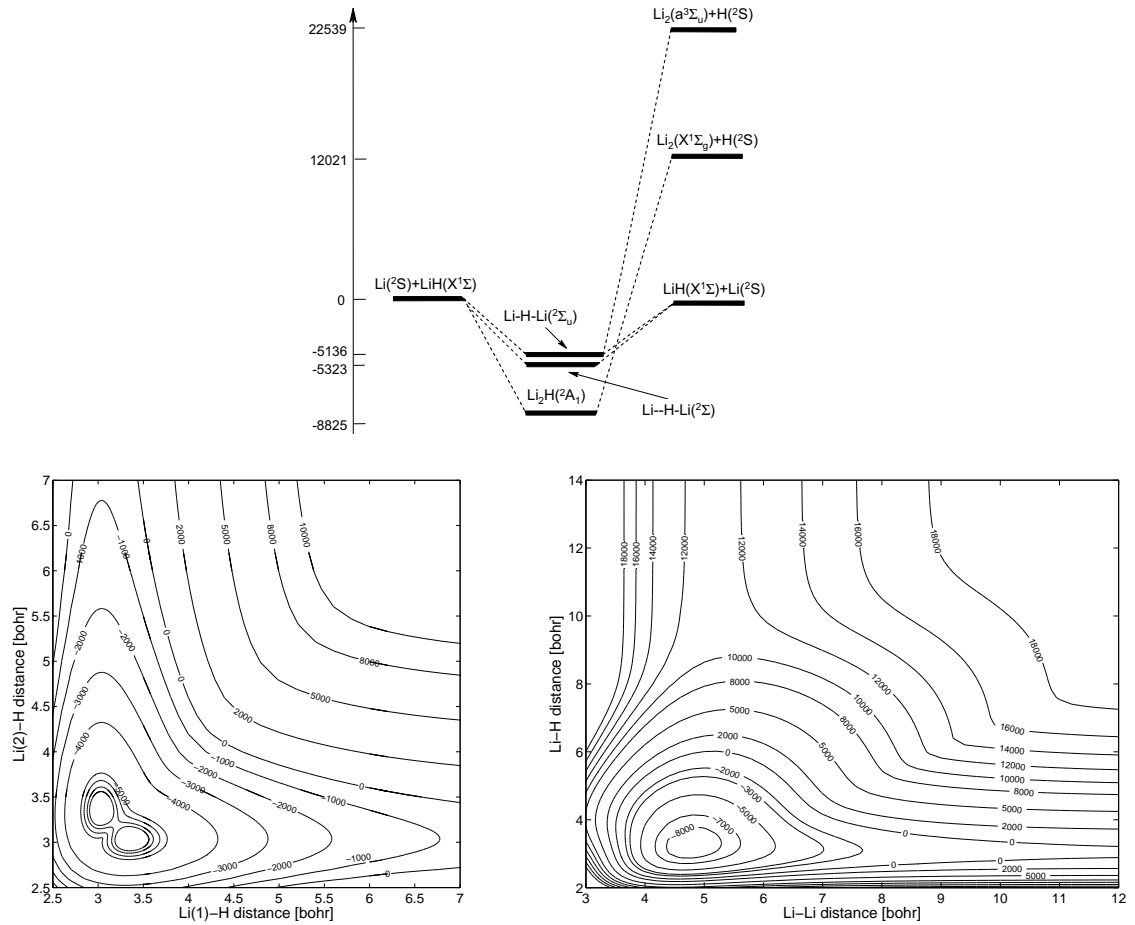


FIG. 9: Schematic representation of the possible reaction pathways in collisions of the lithium atom with the lithium hydride molecule (upper panel), and two-dimensional cuts of the reactive potential energy surfaces for the exchange (left-hand panel) and insertion (right-hand panel) reactions. Energies are in cm⁻¹.

